Modulation of the Association Reaction between Hemoglobin and Carbon Monoxide by Proton and Chloride†

Michele Perrella,*,‡ Marilena Ripamonti,§ and Sonia Caccia‡

Dipartimento di Scienze e Tecnologie Biomediche, University of Milano, Italy, and Istituto di Tecnologie Biomediche Avanzate, CNR, Milano, Italy

Received July 10, 1997; Revised Manuscript Received November 20, 1997

ABSTRACT: A cryogenic technique for the isolation of the ligation intermediates in the association reaction between hemoglobin and carbon monoxide at 20 °C [Perrella, M., Davids, N., and Rossi-Bernardi, L. (1992) *J. Biol. Chem. 267*, 8744−8751] was used to study the effects of proton and chloride concentrations on the rates of the stepwise reactions. The reaction rate was observed to increase continuously in the course of the ligation process, yet the acceleration of the reaction after the binding of two ligand molecules, observed previously in 100 mM KCl, pH 7, was not observed at other pH values. At pH 6.3, such an acceleration occurred after the binding of three ligands, and at pH 8.5, a large acceleration was observed after the binding of the first ligand molecule. Greater CO binding to the β chains was observed under all conditions, as in the previous study. The functional heterogeneity of the chains in the first ligation step increased with pH. The chloride concentration did not influence the distribution of the ligand between the α and β chains at pH 6.3 and 8.5. At pH 7, less binding to the α chains was observed at 7 mM chloride with respect to 100 mM. The nature of the biliganded component isolated at pH 7 in 100 mM KCl and unresolved by the cryogenic technique was studied using a combination of cryogenic and noncryogenic isoelectric focusing. This component was a mixture of intermediates $(\alpha\beta)(\alpha^{CO}\beta^{CO})$, about 65%, and $(\alpha\beta^{CO})(\alpha^{CO}\beta)$, about 35%. The experimental data were compared with the distributions of intermediates calculated according to the Monod kinetic model assuming rapid and concerted transitions between two quaternary structures at each ligation step. The model provided a qualitative fit of the observed distributions of intermediates at acidic and neutral pH. A large discrepancy between the experimental observations and the predictions of the model was found at alkaline pH. The mechanism of the association reaction is discussed in the light of the available information on the tertiary/quaternary structures of the intermediates, as obtained from the studies of the deoxy/cyanomet model of ligation.

Deoxyhemoglobin reacts with the heme ligands to yield 10 species, or intermediates, differing for the state of ligation, type of liganded chain and configuration of the liganded chain in the tetramer, Figure 1. Detailed information is available on the structures and functional properties of the end states. The properties of the intermediates cannot be inferred from those of the end states, unless a two-state mechanism is assumed a priori. The structural properties of the intermediates determine the mechanisms of the reactions, which yield the concentrations of the various species under dynamic and equilibrium conditions. Thus, the intermediates are the key to unlock the mechanisms.

The complexity of the binding process, the intrinsic property of cooperative systems to suppress the concentrations of the intermediates and the technical limitations of traditional approaches have hindered the access to quantitative information on the intermediates in the reactions between hemoglobin and oxygen. Thus, most of the information on the properties of the intermediates has been obtained by the study of the interaction of hemoglobin with nonphysiological

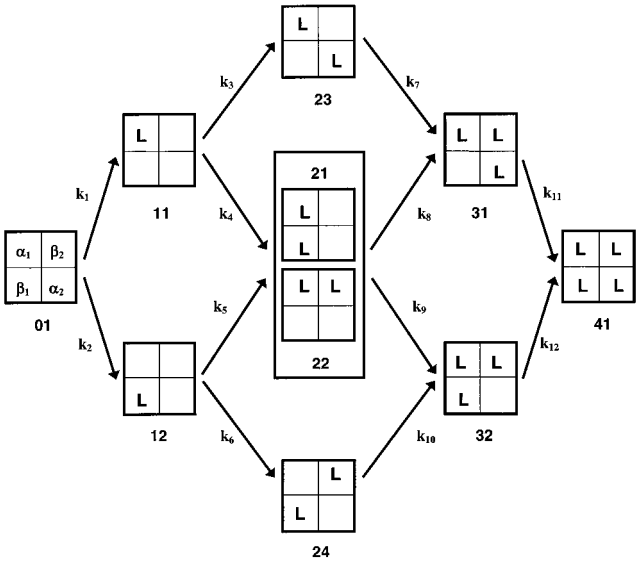

FIGURE 1: Adair scheme of reaction pathways in the association reaction between hemoglobin and ligand L. Species 21 and 22 are enclosed in a box since they are not resolved by the cryogenic technique for the isolation of the intermediates.

† This work was supported by grants from M. U. R. S. T. (60%) and C. N. R., Roma.

* Address correspondence to this author at L. I. T. A., Via Fratelli Cervi, 93−I-20090 Segrate, Milan, Italy.

‡ Dipartimento di Scienze e Tecnologie Biomediche.

§ Instituto di Tecnologie Biomediche Avranzate.

S0006-2960(97)01669-3 CCC: $15.00
Published on Web 02/03/1998

ligands. The cyanide complex of the ferric heme and the metal-substituted hemoglobins have made a direct study of the thermodynamics of cooperative binding and linkage at the various stages of ligation feasible (*1*). The enormous amount of data made available by these studies has greatly expanded our understanding of these processes and confirmed the role of hemoglobin as a paradigmatic case study for protein−protein and protein−ligand interactions.

The interaction of carbon monoxide with hemoglobin is reversible and cooperative with a Hill coefficient similar in value to that measured from the oxygen binding isotherms. We have developed a cryogenic technique to stabilize and analyze the mixture of intermediates in solutions of hemoglobin interacting with CO under dynamic and equilibrium conditions (*2*). This technique does not allow the collection of data as rapidly as the traditional approaches to the study of hemoglobin−ligand interactions, but its unprecedented resolving power and accuracy have contributed to the clarification of several features of these reactions. These studies are complementary to those carried out on the other models of ligation cited above, which exhibit the features of systems under conditions of low cooperativity. The highly cooperative interaction of hemoglobin with carbon monoxide simulates the conditions operating *in vivo.*

In a previous study of the association reaction at 20 °C in 100 mM KCl, pH 7, we have shown that the reaction rate, which increases in a continuous manner, indicates that major conformational changes occur at the diliganded state. Furthermore, the first molecule of ligand binds slightly faster to the β chains than to the α chains. In the presence of IHP,[1] a potent modulator of oxygen affinity that binds hemoglobin in the β chain pocket, the overall rate of the reaction in the first binding step does not change significantly, but the α chains react slightly faster than the β chains (*3*). This observation indicates that the interaction of a modulator with its binding site on one type of chain can influence not only the reactivity toward the homotropic ligand of that chain but also the reactivity of the other type of chain. Thus, the binding of IHP has a 2-fold effect. First, it changes the tertiary structure of the bonded β chains. Second, this change in tertiary structure of the bonded chains promotes a change in the tertiary structure of the α chains not directly involved in the interaction with the modulator. Owing to the relevance of such mechanisms for the understanding of cooperativity and linkage, we have extended our previous studies to other conditions of H^+ and Cl^- concentrations. In addition, we have identified and measured the concentrations of two intermediates, 21 and 22 in Figure 1, which play a key role in the mechanism of cooperativity (*1*) and are not resolved by the cryogenic technique.

The tertiary and quaternary structural changes occurring in the course of the ligation process have been probed recently by two complementary approaches using the deoxy/cyanomet model. Daugherty et al. (*4*) have measured the modulation by proton of the energy of assembling dimers into tetramers at each ligation step. Perrella et al. (*5*) have measured the release of protons by the partially ligated tetramers, known as the Bohr effect. Shibayama et al. (*6*), suspecting that loss of cyanide might have occurred in these studies during the anaerobic incubation of mixtures of deoxy-, cyanomethemoglobin, and hybrid species 21, have expressed criticism. They have shown that the formation of free ferric species promotes a rapid exchange of electrons among the species, which changes the composition of the mixture and makes the studies questionable. Furthermore, Shibayama et al. (*6*) have observed a low concentration of species 21, about 9% relative to the parental species 01, and 41, in experiments in which oxygen was removed slowly from equilibrium mixtures of oxy- and cyanomethemoglobin. Such a low proportion of species 21 disagrees strongly with the nearly statistical values of the concentrations of the same species 21, 01 and 41 obtained by Perrella et al. (*5*) and Daugherty et al. (*4, 7*) under true equilibrium conditions. However, Ackers et al. (*8*) have confirmed that no cyanide depletion occurred under the conditions of the experiments of Perrella et al. (*5*) and Daugherty et al. (*4, 7*) (see also the Results for further comments) and pointed out that the low concentration of species 21 observed in the experiments of Shibayama et al. (*6*) was due to failure to attain true equilibrium.

The studies of Daugherty et al. (*4*) and Perrella et al. (*5*) might provide a possible clue for the interpretation of our findings on the basis of the tertiary/quaternary structural changes undergone by hemoglobin in the process of ligation. Since there is no objective reason to question their validity, in the following, we summarize the main indications from such studies to provide an adequate background for the discussion.

The energetics of the monoliganded intermediates indicates that these species are in T structure at all pH values. The pH profiles of the Bohr effect of these species are consistent with the energetics. The diliganded species 22, 23, and 24 (Figure 1) are in R state according to the energetics. The observed changes in the Bohr effect with pH of these species are consistent with an interpretation of such effects as due to tertiary structural changes within the R state. The energetics and the pH profile of the Bohr effect of intermediate 21 are different from those of intermediate 22, despite them both having one α and one β liganded chain. The energetics indicates a T structure for intermediate 21 as for the monoliganded species. The pH profile of the Bohr effect of intermediate 21, however, is not equivalent to the sum of the pH profiles of the two monoliganded species. This finding is consistent with the analysis of the energetics of species 21, which indicates cooperativity in binding the ligand within the dimeric half-molecule. The triliganded species are in quaternary R state according to the energetics. The significant amount of Bohr protons released upon oxygenation by these species at neutral and acidic pH, whereas at pH above 8 no Bohr effect is observed, indicates that the tertiary structures of the unliganded chains in the R quaternary structure vary with pH, as observed for the diliganded species 22, 23, and 24. In conclusion, the tertiary structures of the chains within each quaternary structure are influenced by the conditions, e.g., pH. The interactions of the homotropic ligands with the protein control both the tertiary structures of the chains and the quaternary structure of the tetramer. The heterotropic ligands influence the

[1] Abbreviations: IHP, inositolhexaphosphate; 2,3-DPG, 2,3-diphosphoglycerate; EGOH, ethyleneglycol; FeCy, ferricyanide; HbCO, carboxyhemoglobin; Hb, deoxyhemoglobin. All rate constants are microscopic constants and concentrations are on a heme basis.

tertiary structures of the chains within each quaternary structure.

MATERIALS AND METHODS

Hemoglobin Preparation. Hemoglobin A_0 was purified by chromatography from red blood cell lysates (*3*). Stock solutions (15 g/dL) in 5 mM and 100 mM KCl, pH 7, were stored in liquid nitrogen. To prepare deoxygenated hemoglobin for the reactions with CO at pH 6.3 ± 0.05, samples of the stock solutions were titrated with 0.1 M HCl, diluted with distilled water or 100 mM KCl to the final protein concentration and equilibrated with N_2 by tonometry. The average [Cl^-] in the experiments carried out at low chloride concentration was 7 ± 2 mM. To prepare deoxygenated hemoglobin at pH 8.5 ± 0.1, samples at pH 7 in 5 mM or 100 mM KCl were equilibrated with N_2. The pH was then adjusted by the addition of suitable amounts of deoxygenated 0.1 M KOH in 5 mM or 100 mM KCl, respectively. All samples were stabilized against auto-oxidation by the addition of catalase and superoxide dismutase. After equilibration with N_2, traces of O_2 were removed from the hemoglobin solution by the addition of dithionite (5 μmol/mL).

Isolation of the Intermediates. The cryogenic technique for the isolation, identification and quantitation of the CO intermediates is described in detail in previous works (*2, 3*). Briefly, to trap the intermediates a solution deoxyhemoglobin (≥1 mM, heme concentration) is mixed rapidly with a substoichiometric solution of CO (0.9 mM) and after 100 ms the mixture (200−300 μL) is injected into a stirred anaerobic cryosolvent, 1 mL of 60% (v/v) EGOH/water, containing phosphate (10 mM) and a 10-fold excess of FeCy with respect to Hb and cooled at −30 °C. Under these conditions, all CO binds to hemoglobin, no significant dissociation of CO occurs and only the unliganded chains are quantitatively oxidized to the ferric state (*2*). This chemical and thermal quenching procedure stabilizes the intermediates with regard to the redistribution of the ligand among the chains and the exchange of dimers among the various partially oxidized tetramers. The pH of the 22 mM phosphate solution used to prepare the cryogenic mixture was 7.5 for experiments using hemoglobin samples at neutral or acidic pH and 6.5 for hemoglobin samples at alkaline pH. The mixture of oxidized intermediates was then separated by cryofocusing at −25 °C on gel tubes, and the hemoglobin components excised from the gel tubes were assayed by the pyridine hemochromogen method after elution from the gel. Two intermediates isolated by this technique as a single component are shown in Figure 1 enclosed in a box.

Analysis of the Hemoglobin Components Isolated by Cryofocusing. Samples of solutions of partially oxidized HbCO, prepared and stored as a standard, or of solutions containing CO intermediates, as trapped by the procedure described above, were cryofocused. The gels were then removed from the glass tubes, sliced in correspondence to the isolated components and 5−10 slices containing the same component were placed on the slot of a gel plate for IEF at 15 °C. Before loading the gel plate, the slices, still containing the solvent used for cryofocusing, were kept under CO in a glass vial cooled at −15 °C to slow the denaturation and auto-oxidation of the protein. The slots of the plate were filled with a solution of ampholines, pH range 7−9,

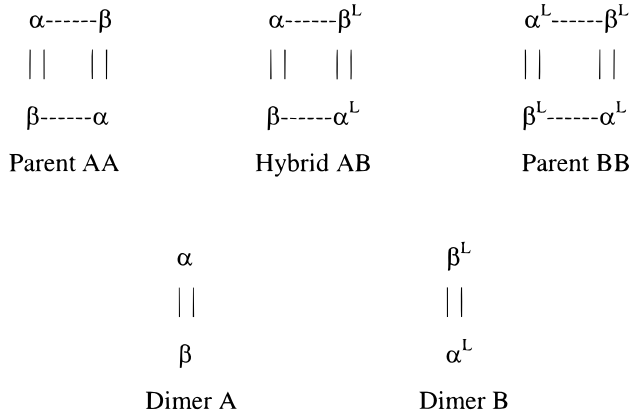

FIGURE 2: Schematic representation of the dimer exchange reactions between two parental symmetrical species AA and BB yielding an asymmetrical hybrid AB.

containing catalase and superoxide dismutase and saturated with CO. IEF was then carried out for 3−4 h, starting at 30 V/cm and ending the run at 80 V/cm. At the end of the run, the hemoglobin zones on the plate were stained with Coomassie Blue fast stain. Alternatively, the hemoglobin zones were excised from the gel and the protein eluted in 10 mM phosphate and 10 mM KCl, pH 7, was assayed using the pyridine hemochromogen method.

Data Analysis. The data on the concentrations of the intermediates were determined by the cryogenic procedure after the complete binding of CO to hemoglobin and before any significant dissociation of the ligand. Thus, the data shown in this work do not vary with the time course of the reaction, but with the total amount of bound CO. The concentrations of the intermediates obtained at each value of total CO bound to hemoglobin depend on the values of the rates along the pathways in Figure 1. Numerical methods of analysis, based on the Finite Element approach, were used to calculate the values of the parameters ($\leq n - 1$) in a kinetic scheme containing n rate constants. One parameter was assigned an arbitrary or published value (*9*). Two kinetic schemes were used for the analysis, (1) a kinetic scheme of four consecutive reactions assuming no functional heterogeneity of the intermediates in the same state of ligation [this scheme allows for three adjustable parameters, l_1', l_2', and l_3', assuming $l_4' = 6.0\ \mu M^{-1}\ s^{-1}$ (*10, 11*)]; (2) a kinetic scheme, such as the one shown in Figure 1, assuming a number of adjustable parameters varying from 5 to 11 and at least one fixed value constant, such as k_{11} or $k_{12} = 6.0\ \mu M^{-1}\ s^{-1}$. As a result of the error in the determination of the concentrations of several intermediates, as high as 100% of the concentration values (*3*), and the very low values of the concentrations of some intermediates, fitting 11−10 adjustable rate constants to the data of this work yielded negative values for some of the parameters. Thus, constrained forms of the scheme in Figure 1 had to be used (Figure 8).

Monod Kinetic Model. The concentrations of the intermediates formed in the association reaction under the conditions of the experiments reported in this paper were calculated assuming a concerted transition of hemoglobin between two quaternary structures (*12, 13*). The basic assumptions were as follows. At each pH value, the T and R structures are characterized by unique values for the microscopic rate constants for the association, k_T' and k_R',

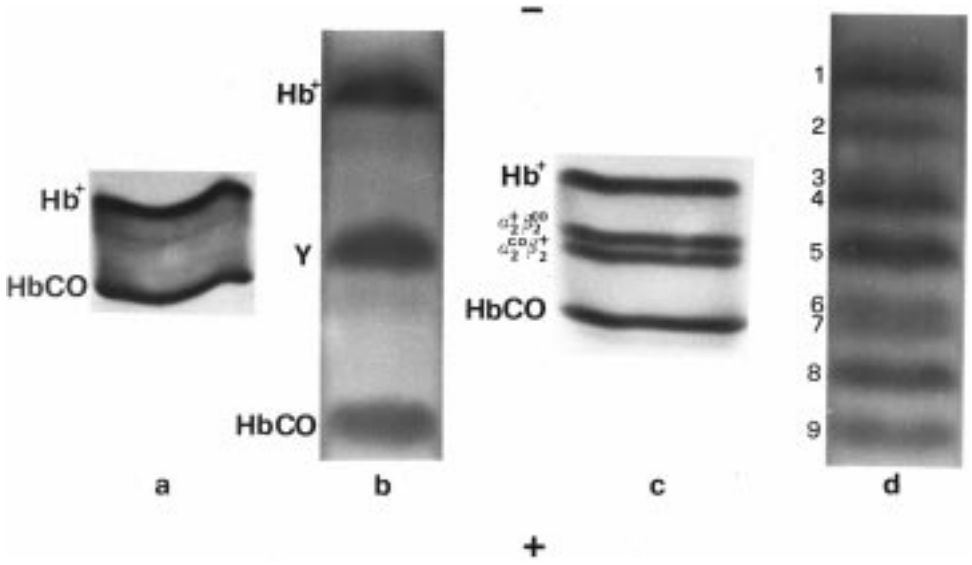

FIGURE 3: Noncryogenic versus cryogenic separations of mixtures of hemoglobin species. (a) IEF at 15 °C on a gel slab, containing ampholines pH range 6−8, of a one-to-one mixture of Hb^+ and HbCO; (b) cryofocusing at −25 °C on a gel tube of the same mixture as in panel a; (c) IEF at 15 °C on a gel slab, containing ampholines pH range 7−8, of a sample of HbCO 50% oxidized by FeCy; (d) cryofocusing at −25 °C on a gel tube of the same mixture as in panel c. The nine components in panel d are identified in Table 2.

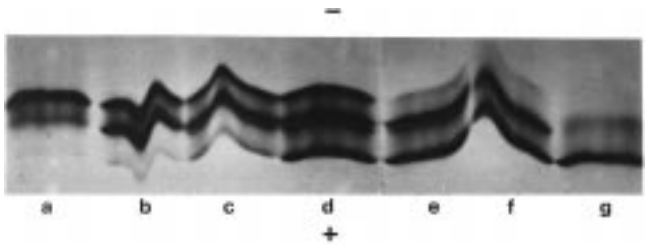

FIGURE 4: IEF at 15 °C on a gel slab, containing ampholines pH range 6−8, of some of the components in Figure 3d, isolated by cryofocusing at −25 °C, a sample of 50% oxidized HbCO and identified in Table 2. Five slices containing the component excised from the gel tube used for cryofocusing were loaded on each gel slot (a−g). The components loaded on each slot and the main species obtained by disproportionation of the components are (from cathode to anode): (a) component n° 1, Hb^+; (b) component n° 2, Hb^+, and $(\alpha^+\beta^{CO})(\alpha^+\beta^{CO})$; (c) components n° 3 and 4, Hb^+, $(\alpha^+\beta^{CO})(\alpha^+\beta^{CO})$, and $(\alpha^{CO}\beta^+)(\alpha^{CO}\beta^+)$; (d) component n° 5, Hb^+, $(\alpha^+\beta^{CO})(\alpha^+\beta^{CO})$, $(\alpha^{CO}\beta^+)(\alpha^{CO}\beta^+)$, and HbCO; (e) components n° 6 and 7, $(\alpha^+\beta^{CO})(\alpha^+\beta^{CO})$, $(\alpha^{CO}\beta^+)(\alpha^{CO}\beta^+)$, and HbCO; (f) component n° 8, $(\alpha^{CO}\beta^+)(\alpha^{CO}\beta^+)$, and HbCO; (g) component n° 9, HbCO.

and dissociation, k_T and k_R, reactions:

$$T_{(i-1)} + CO \xrightarrow{g'k_T'} T_i$$

$$T_i \xrightarrow{gk_T} T_{(i-1)} + CO$$

$$R_{(i-1)} + CO \xrightarrow{g'k_R'} R_i$$

$$R_i \xrightarrow{gk_R} R_{(i-1)} + CO \qquad (1)$$

where g' and g are statistical weight-factors: $g' = 4, 3, 2$, and 1 and $g = 1, 2, 3$, and 4 for $i = 1, 2, 3$, and 4.

At each ligation step the equilibration of the liganded species between the two quaternary structures, T and R, occurs more rapidly than the binding of the next CO molecule. Thus, the proportions of intermediates in T and R structure, $f_i = [T_i]/([T_i] + [R_i])$ and $(1 - f_i)$, respectively,

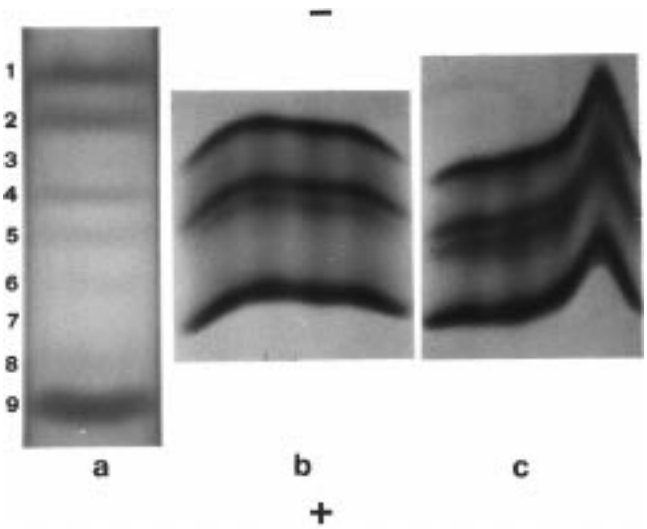

FIGURE 5: Cryofocusing separation at −25 °C on a gel tube of the intermediates in the association reaction between hemoglobin and CO in 100 mM KCl, pH 7, yielding about 50% CO saturation. (a) The nine components are identified in Table 2; (b and c) IEF at 15 °C on a gel slab, containing ampholines pH range 7−8, of component n° 5 excised from the gel tube. Identity of the species from cathode to anode: Hb^+, $(\alpha^+\beta^{CO})(\alpha^+\beta^{CO})$, $(\alpha^{CO}\beta^+)(\alpha^{CO}\beta^+)$, and HbCO.

for $i = 1-4$, can be calculated knowing the values of the allosteric constant, $L = [T_0]/[R_0]$, and the ratio, c, of the affinities for the ligand of the two structures, K_T and K_R, since

$$f_i = Lc^i/(1 + Lc^i) \qquad (2)$$

The kinetics of the model can be described by four consecutive reactions caracterized by the following rate costants:

$$k'_i = g'[f_{(i-1)}k'_T + (1 - f_{(i-1)})k'_R] \qquad (3)$$

$$k_i = g[f_i k_T + (1 - f_i)k_R] \qquad (4)$$

$$i = 1, 2, 3, 4$$

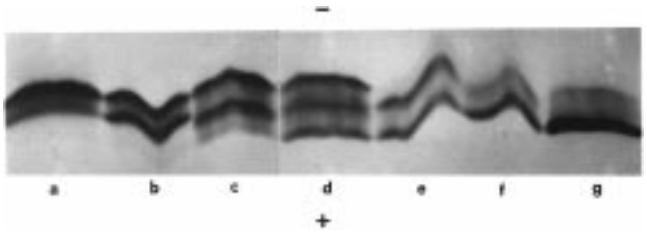

FIGURE 6: IEF at 15 °C on a gel slab, containing ampholines pH range 6−8, of the products of disproportionation of some of the intermediates isolated by cryofocusing at −25 °C as in Figure 5a. The components are identified in Table 2. Ten slices containing the component excised from the gel tube used for cryofocusing were loaded onto each gel slot (a−g). The components loaded onto each slot and the species obtained by disproportionation of the components from cathode to anode are: (a) component n° 1, Hb^+; (b) component n° 2, Hb^+ and $(\alpha^+\beta^{CO})(\alpha^+\beta^{CO})$; (c) component n° 4, Hb^+ and $(\alpha^{CO}\beta^+)(\alpha^{CO}\beta^+)$; (d) component n° 5, Hb^+, $(\alpha^+\beta^{CO})$-$(\alpha^+\beta^{CO})$, $(\alpha^{CO}\beta^+)(\alpha^{CO}\beta^+)$ and HbCO; (e), Component n° 6, $(\alpha^+\beta^{CO})(\alpha^+\beta^{CO})$, and HbCO; (f) component n° 8, $(\alpha^{CO}\beta^+)(\alpha^{CO}\beta^+)$ and HbCO; (g) component n° 9, HbCO. A better resolution of component n° 5 on a gel slab containing ampholines pH range 7−8 is shown in Figure 5, panels b and c.

The numerical solution of the system of differential equations was carried out using the Matlab 4.0 software. Values of K_R were calculated assuming the association and dissociation rate constants $l_4' = 6.0\ \mu M^{-1}\ s^{-1}$ and $l_4 = 0.011\ s^{-1}$ at 20 °C, respectively, invariant with pH (*11*, *14*). Values of K_T were calculated from the association rate constants l_1' listed in Table 4 and the dissociation rate constants l_1 of Samaja et al. (*14*) and Sharma et al. (*15*, *16*). Table 1 lists some values of L as determined from oxygen equilibrium isotherms by Imai (*17*) and Chu and Ackers (*18*) and from the carbon monoxide equilibrium data of Perrella et al. (*19*). The values of c, determined from the above data on the rate constants and used for the calculations, were 4.17 ± 10^{-3} at pH 6, 1.59 ± 10^{-3} at pH 7 [1.53 ± 10^{-3} from the data of Perrella et al. (*19*)] and 18.1 ± 10^{-3} at pH 8.5. The assumption of the Monod kinetic model, i.e., the rapid attainment of the T/R equilibrium at each ligation step before the binding of the next CO molecule, may not hold true under all conditions in our CO binding experiments. However, the distributions of intermediates calculated assuming published values of the rates of the T/R interconversion (*20*, *21*) were close to those calculated using the assumption of the model.

RESULTS

Hybridization and Disproportionation Reactions of the Oxidation Intermediates. Figure 2 gives a schematic representation of such reactions. Parental species AA, e.g., Hb^+ and BB, e.g., HbCO, yield the hybrid AB, namely $(\alpha^+\beta^+)$-$(\alpha^{CO}\beta^{CO})$ by exchanging the dimers. The exchange reactions occur rapidly and reversibly at temperatures above zero.

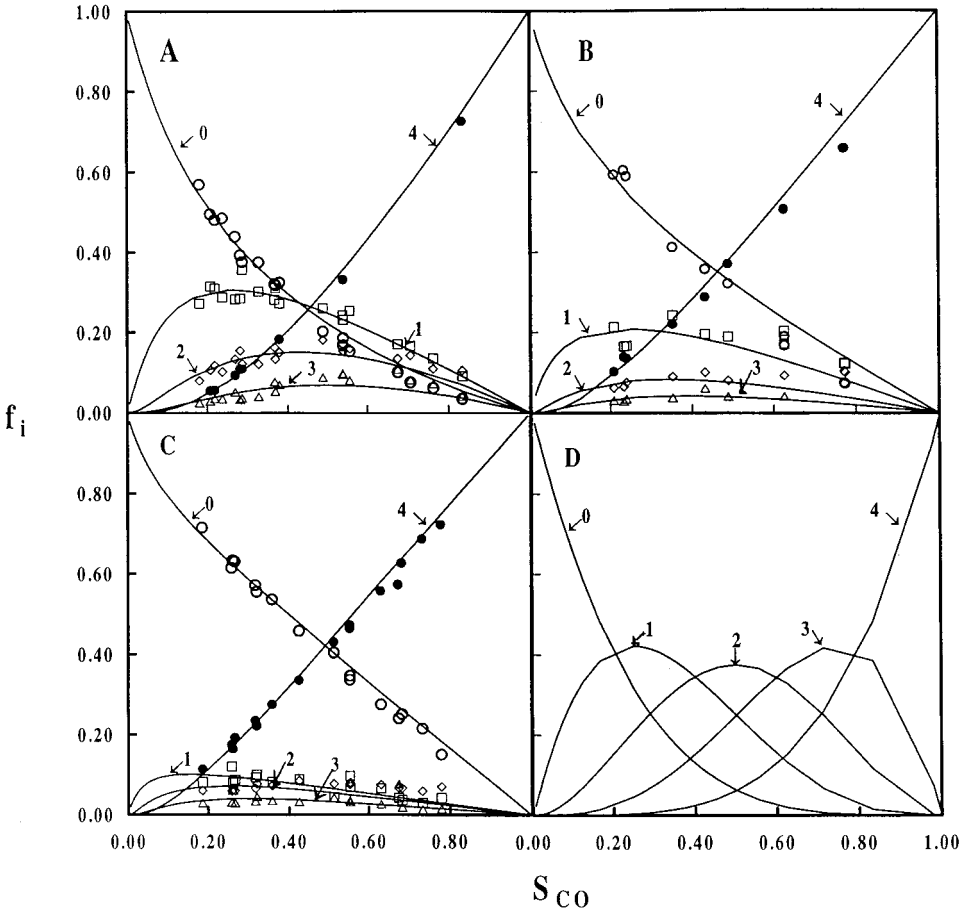

FIGURE 7: Fractional values of the concentrations of the species formed in the association reaction versus total fractional value of bound CO. Hb, (○); HbCO, (●); sum of intermediates 11 and 12 (Figure 1) (□); sum of intermediates 21, 22, 23, and 24 (◇); sum of intermediates 31 and 32 (△). (A) Data at pH 6.3 in 7 and 100 mM KCl; (B) data at pH 7 in 7 mM KCl; (C) data at pH 8.5 in 7 and 100 mM KCl; lines fitted according to a four rate constant scheme of consecutive reactions, l_1', l_2', l_3', l_4', assuming $l_4' = 6.0\ \mu M^{-1}\ s^{-1}$ under all conditions (11); (D) statistical distributions of intermediates in the association reaction calculated assuming $l_1' = l_2' = l_3' = l_4'$. The state of ligation of the intermediates for each line is indicated by the respective arrows.

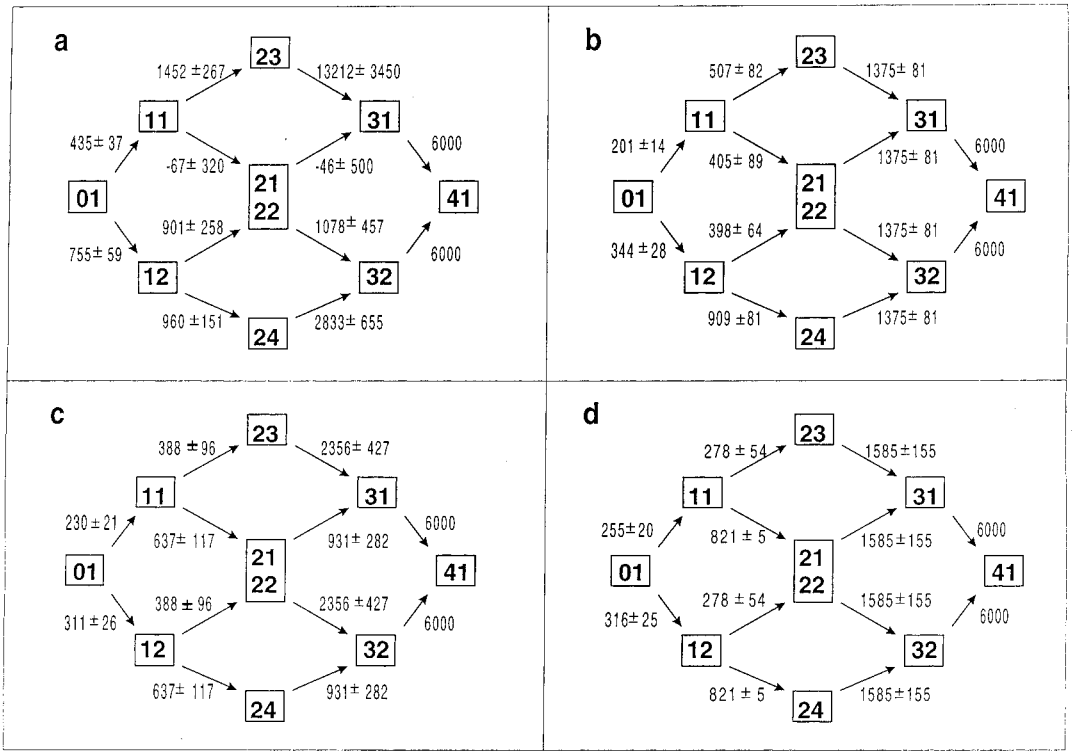

FIGURE 8: Analyses of the data on the concentrations of the intermediates in the association reaction at pH 6.3, 7, and 100 mM KCl, according to various constrained forms of the scheme in Figure 1 and assuming $k_{11} = k_{12} = 6000$ mM^{-1} s^{-1} in all cases. Adjustable parameters: (A), k_1, k_2, k_3, k_5, k_4, k_6, k_7, k_9, k_8, k_{10}; (B) k_1, k_2, k_3, k_5, k_4, k_6, $k_7 = k_9 = k_8 = k_{10}$; (C) k_1, k_2, $k_3 = k_5$, $k_4 = k_6$, $k_7 = k_9$, $k_8 = k_{10}$. (D) k_1, k_2, $k_3 = k_5$, $k_4 = k_6$, $k_7 = k_9 = k_8 = k_{10}$.

Table 1: Values of *L*, the Allosteric Constant (*12*), at 20−25 °C from Various Sources[a]

	L		
pH	Imai (*17*)	Chu and Ackers (*18*)	Perrella et al. (*19*)
6.3	(1.12×10^6)	(1.12×10^9)	
6.5	6.2×10^5		
7.0	(2.11×10^5)	(7.87×10^7)	2.05×10^7
7.4	8.7×10^4	1.15×10^7	
8.0		1.02×10^7	
8.5	9.26×10^3	2.49×10^5	
8.95		1.58×10^4	

[a] The values obtained by extrapolation are in brackets.

Under these conditions, IEF detects only two components, i.e., the parental species. The three components can be detected by cryofocusing, since at subzero temperatures the tetramer dissociation reactions are slow. The case of the hybridization reactions is illustrated in Figure 3. A 1:1 mixture of Hb^+ and HbCO was focused at 15 °C yielding a pattern of two major components (Figure 3a). The same sample injected into a cryosolvent at −25 °C and cryofocused at this temperature yielded a pattern of three major components (Figure 3b). The minor components appearing in Figure 3b are the products of hybridization of Hb^+ and HbCO with trace amounts of species $(\alpha^+\beta^{CO})(\alpha^+\beta^{CO})$ and $(\alpha^{CO}\beta^+)$-$(\alpha^{CO}\beta^+)$, which contaminate the sample. This is shown more clearly in Figure 3, panels c and d. A solution of HbCO, 50% oxidized by FeCy, yielded four components when focused at 15 °C (Figure 3c) and, at −25 °C, nine components (Figure 3d), which are the products of hybridization of the four parental species shown in Figure 3c. In principle, 10 components in statistical proportions should be obtained at −25 °C. However, hybrids $(\alpha^+\beta^+)(\alpha^{CO}\beta^{CO})$ and $(\alpha^+\beta^{CO})(\alpha^{CO}\beta^+)$ have identical isoelectric points and cannot be resolved. The nine components in Figure 3d are listed and identified in Table 2, first column, according to a simple procedure (*2*) suggested by the observation that, at equilib-

Table 2: Identification of the Components Isolated by Cryofocusing[a]

component from cryofocusing	Gel slot for IEF at 15 °C	Species from IEF at 15 °C
1[Hb^+]	(a)	Hb^+ $(\alpha^+\beta^{CO})(\alpha^+\beta^{CO})$ (traces)
2 [$(\alpha^+\beta^{CO})(\alpha^+\beta^+)$]	(b)	**Hb^+** **$(\alpha^+\boldsymbol{\beta}^{CO})(\alpha^+\boldsymbol{\beta}^{CO})$** HbCO (traces)
3 [$(\alpha^+\beta^{CO})(\alpha^+\beta^{CO})$] 4 [$(\alpha^{CO}\beta^+)(\alpha^+\beta^+)$]	(c)	$(\alpha^+\beta^{CO})(\alpha^+\beta^{CO})$ **Hb^+** **$(\alpha^{CO}\boldsymbol{\beta}^+)(\alpha^{CO}\boldsymbol{\beta}^+)$** HbCO (traces)
5 [$(\alpha^+\beta^+)(\alpha^{CO}\beta^{CO})$] [$(\alpha^{CO}\beta^+)(\alpha^+\beta^{CO})$]	(d)	**Hb^+** **$(\alpha^+\boldsymbol{\beta}^{CO})(\alpha^+\boldsymbol{\beta}^{CO})$** **$(\alpha^{CO}\boldsymbol{\beta}^+)(\alpha^{CO}\boldsymbol{\beta}^+)$** **HbCO**
6 [$(\alpha^{CO}\beta^{CO})(\alpha^+\beta^{CO})$] 7 [$(\alpha^{CO}\beta^+)(\alpha^{CO}\beta^+)$]	(e)	Hb^+ (traces) **$(\alpha^+\boldsymbol{\beta}^{CO})(\alpha^+\boldsymbol{\beta}^{CO})$** $(\alpha^{CO}\beta^+)(\alpha^{CO}\beta^+)$ **HbCO**
8 [$(\alpha^{CO}\beta^+)(\alpha^{CO}\beta^{CO})$]	(f)	Hb^+ (traces) **$(\alpha^{CO}\boldsymbol{\beta}^+)(\alpha^{CO}\boldsymbol{\beta}^+)$** **HbCO**
9 [HbCO]	(g)	$(\alpha^+\beta^{CO})(\alpha^+\beta^{CO})$ (traces) $(\alpha^{CO}\beta^+)(\alpha^{CO}\beta^+)$ (traces) HbCO

[a] First column: species separated by cryofocusing a sample of partially oxidized HbCO (Figure 3d); second column: slots on the gel plate in Figure 4 (a−g); third column: products of disproportionation (bold character) of the species isolated by cryofocusing, Figure 3D, refocused at 15 °C, Figure 4 (a−g).

Table 3: Relative Proportions of Intermediates 21 and 22 Isolated in the Association Reaction in 100 mM KCl, pH 7, and at Various Values of CO Saturation

S_{CO} %	[21] (%)	[22] (%)
35.5	62	38
42.7	59	41
52.5	59	41
55.1	61	39
67.7	69	31
71.8	66	34

rium, the focusing position of the hybrid in a linear gradient is midway between those of the parental species (*22*). It should be noted that cyanide binding to the ferric chains cancels out the charge differences among the species. In the presence of a saturating concentration of cyanide, the components in Figure 3d cofocus with component *n*° 9, that is, HbCO. Incomplete saturation by cyanide restores the pattern of nine components. Thus, depletion of cyanide during the incubation of the deoxy/cyanomet intermediates in the experiments of Daugherty et al. (*7*) and Perrella et al. (*5*), as suspected by Shibayama et al. (*6*), would have been monitored by the cryofocusing technique they used for the analyses of the equilibrium mixtures.

A more elaborate procedure for the identification of the hybrids in Figure 3d makes use of the disproportionation reactions of the hybrids at temperatures above zero. Figure 4 (panels a−g) shows the pattern of species obtained by refocusing at 15 °C on a gel slab the protein components excised from gels used for cryofocusing the sample of partially oxidized HbCO, as in Figure 3d. Since components 3 and 4 and components 6 and 7 in Figure 3d partially overlap, they were excised together. Listed in Table 2, third column, are the identities of the separated parental species for each gel slot, second column.

Minor bands appearing on the gel in Figure 4 (panels a−g) were the result of physical contamination by adjacent components in the process of gel slicing and of slight autooxidation of the CO-liganded chains exposed to oxygen. A quantitative assay was carried out to check whether the parental species, produced by disproportionation, were in the expected 1:1 ratio. Typically, the analysis of the protein loaded on slot b in Figure 4 yielded 46.2% Hb^+, 52.1% $\alpha_2^+\beta_2^{CO}$, and 1.7% HbCO. It cannot be excluded that traces of HbCO observed in Figure 4 (panels b and c), and similarly of Hb^+ observed in Figure 4 (panels e and f), could also be due to heme exchange and electron-transfer reactions before and during IEF. However, the finding that the ratios of the parental species were close to the expected value, as in the example quoted above, indicates that the effects of these reactions were of minor importance.

Resolution of the Mixture of Intermediates 21 and 22 in the CO Association Reaction. The cryogenic technique does not resolve intermediates 21 and 22, which upon oxidation by FeCy, yield the species with identical isoelectric points $[21]_{ox}$, i.e., $(\alpha^+\beta^+)(\alpha^{CO}\beta^{CO})$, and $[22]_{ox}$, i.e., $(\alpha^{CO}\beta^+)(\alpha^+\beta^{CO})$. The disproportionation reactions illustrated in the preceding section provide a solution to this problem. Species $[21]_{ox}$ disproportionates at 15 °C yielding Hb^+ and HbCO. Species $[22]_{ox}$ disproportionates to yield species $(\alpha^+\beta^{CO})(\alpha^+\beta^{CO})$ and $(\alpha^{CO}\beta^+)(\alpha^{CO}\beta^+)$. Thus, the component unresolved by cryofocusing, when eluted from the gel and refocused at 15 °C, should yield the bands of Hb^+ and HbCO, if it contains species $[21]_{ox}$, or the bands of $(\alpha^+\beta^{CO})(\alpha^+\beta^{CO})$ and $(\alpha^{CO}\beta^+)$-$(\alpha^{CO}\beta^+)$, if it contains species $[22]_{ox}$. If both species are present, all four bands are obtained. The relative amounts of Hb^+ plus HbCO and $(\alpha^+\beta^{CO})(\alpha^+\beta^{CO})$ plus $(\alpha^{CO}\beta^+)(\alpha^{CO}\beta^+)$ depend on the proportions of intermediates 21 and 22 formed in the association reaction between Hb and CO.

Figure 5a shows the separation by cryofocusing of the intermediates in the association reaction at about 50% CO saturation. Nine components are observed, as for the separation of the standard sample of partially oxidized HbCO in Figure 3d. The identification of the components is also the same (Table 2). Notable is the difference in the concentrations of the oxidized intermediates between the sample in Figure 3d, which contains species in statistical proportions, and the sample in Figure 5a, in which Hb^+, the product of oxidation of Hb, and HbCO predominate over all the other species due to the cooperativity in the association reaction. As a result of the low concentrations of the intermediates and the low protein content of the sample, components 3 and 4 and 6 and 7, which overlap in Figure 3d, are resolved in Figure 5a. The main components in Figure 5a were excised and refocused at 15 °C yielding the pattern of Figure 6 (panels a−g). Such a pattern is the same as that in Figure 4 (panels a−g) except that the products of disproportionation of component 4 in Figure 6c are not contaminated by component 3. Similarly, the products of disproportionation of component 6 in Figure 6e are not contaminated by component 7.

Figure 5, panels b and c, shows details of the disproportionation products of component 5 from two experiments of isolation of the intermediates in the association reaction in 100 mM KCl, pH 7. Four species, Hb^+, $(\alpha^+\beta^{CO})(\alpha^+\beta^{CO})$, $(\alpha^{CO}\beta^+)(\alpha^{CO}\beta^+)$, and HbCO, were obtained. The amount of Hb^+ plus HbCO was systematically greater than the amount of $(\alpha^+\beta^{CO})(\alpha^+\beta^{CO})$ plus $(\alpha^{CO}\beta^+)(\alpha^{CO}\beta^+)$ (Table 3). This indicates that both intermediates 21 and 22 were formed in the association reaction, albeit in different concentrations.

Effects of H^+ and Cl^- on the Distribution of the Intermediates. The concentrations of the intermediates were obtained at two different values of chloride concentration, 7 and 100 mM, at pH 6.3 and 8.5, and at 7 mM chloride at pH 7. The data at 100 mM chloride, pH 7, shown here were obtained partly in a previously published work (*3*) and partly in this work (Table 3). Since the data in 7 and 100 mM chloride were not significantly different at pH 6.3 and 8.5, such data were pooled.

Scheme of four Consecutive Reactions. Ignoring the slight functional heterogeneity of the intermediates in the same state of ligation, Figure 7 (panels a−c) shows the fractional values of the concentrations of Hb, HbCO and total concentrations of mono-, di-, and triliganded intermediates obtained at pH 6.3, 7, and 8.5 as a function of the fractional value of bound CO. The lines in Figure 7 (a−c) were obtained by fitting the data according to a four rate constant model, assuming $l_4' = 6.0\ \mu M^{-1}\ s^{-1}$ at all pH values (*11*). The values of the fitted constants are listed in Table 4. The distributions of intermediates calculated for $l_1' = l_2' = l_3' = l_4'$, that is in the absence of cooperativity, are plotted in Figure 7d. The calculated ratios of the rate constants, l_n'/l_{n-1}', which are useful for a discussion of the mechanism, are listed in Table 5.

Table 4: Rate Constants Fitted to the Data in Figure 7 (a−c) According to a Model of Four Consecutive Reactions Assuming $l_4' = 6\ \mu M^{-1}\ s^{-1}$ (*11*)[a]

l_n' ($\mu M^{-1}\ s^{-1}$)	pH			
		[Cl⁻] = 7 (mM)	[Cl⁻] = 100[b] (mM)	
	6.2	7	7	8.5
l_1'	0.273 ± 0.023	0.116 ± 0.025	0.113 ± 0.011	0.0888 ± 0.008
l_2'	0.516 ± 0.045	0.415 ± 0.092	0.265 ± 0.026	0.858 ± 0.087
l_3'	1.40 ± 0.139	1.51 ± 0.394	1.47 ± 0.170	1.70 ± 0.197

[a] Data at 7 and 100 mM chloride were pooled except at pH 7, as indicated. [b] Data from Perrella et al. (*3*).

Table 5: Ratios l_n'/l_{n-1}' of the Stepwise Rate Constants for CO Binding According to a Mechanism of Four Consecutive Reactions and l_4'/l_1' at Different pH Values[a]

	pH			
	6.3	7 ([Cl⁻] = 7 mM)	7 ([Cl⁻] = 100 mM)[b]	8.5
l_2'/l_1'	1.89 ± 0.23	3.58 ± 1.11	2.34 ± 0.32	9.66 ± 1.31
l_3'/l_2'	2.70 ± 0.36	3.63 ± 1.24	5.55 ± 0.84	1.98 ± 0.31
l_4'/l_3'	4.30 ± 0.43	3.98 ± 1.04	4.08 ± 0.47	3.53 ± 0.41
l_4'/l_1'	22.0 ± 1.8	51.7 ± 11.1	53.1 ± 5.2	67.6 ± 6.1

[a] Ratios calculated from the data listed in Table 4. [b] Data from Perrella et al. (3).

Schemes of Multiple Pathways of Reaction. A significant difference between the concentrations of species in the same state of ligation was observed for the monoliganded intermediates, as shown in Figure 9. The concentrations of intermediates 23 and 24 and the concentrations of intermediates 31 and 32 were similar within the error. A difference between the sum of the concentrations of the diliganded intermediates along the peripheral pathway in Figure 1, that is 23 plus 24, and the sum of the diliganded intermediates along the central pathway, that is 21 plus 22, could be indicative of functional heterogeneity among these intermediates, particularly between species 21 and 22. However, the observed difference was not significant. Only the analysis by noncryogenic techniques of the mixture of the products of the oxidation of intermediates 21 and 22 yielded clear evidence of a slight functional heterogeneity of these two species. However, since the observed difference in the concentrations of species 21 and 22 by this procedure was less than the error in the determination of the concentrations of the intermediates, it was not possible to make use of such an information to obtain significant values of the relevant rate constants of the association reactions. Figure 8 shows the analysis of the data at pH 6.3 according to the scheme of Figure 1. Figure 8 (panels b−d) summarizes the results of the analyses using constrained kinetic schemes, which could provide information on the functional heterogeneity of the α and β subunits. All of them agreed in indicating faster binding to the β chains in the first ligation step with a value of the ratio k_2/k_1 in the range 1.2−1.7 and failed to provide information with regard to the next binding steps. The data at pH 7, in 7 and 100 mM KCl (from previously published work), and pH 8.5 were analyzed similarly yielding evidence of a significant functional heterogeneity of the α and β chains in the first ligation step. To compare the values of the ratio k_2/k_1, as obtained under the various conditions, the scheme of Figure 8d with five adjustable parameters (k_1, k_2, $k_3 = k_5$, $k_4 = k_6$, $k_7 = k_9 = k_8 = k_{10}$) was used. The results are listed in Table 6. The same scheme was used to calculate the distributions of α and β chain monoliganded intermediates, shown as the lines fitting the concentrations of such intermediates in Figure 9, panels a−c.

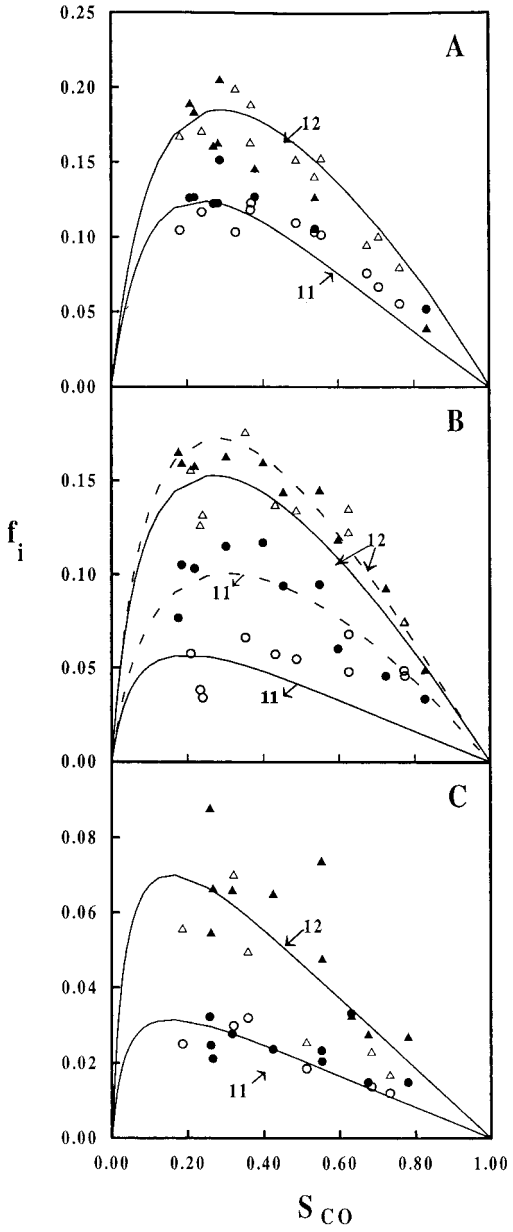

FIGURE 9: Concentrations of the α monoliganded (circles) and β monoliganded (triangles) intermediates in 7 mM KCl (open symbols) and 100 mM KCl (closed symbols). (A) pH 6.3; (B) pH 7; (C) pH 8.5. The lines were fitted assuming the kinetic scheme depicted in Figure 8D (k_1, k_2, $k_3 = k_5$, $k_4 = k_6$, $k_7 = k_9 = k_8 = k_{10}$ adjustable constants and $k_{11} = k_{12} = 6.0\ \mu M^{-1}\ s^{-1}$). In panel B, the full and dashed lines fit the data at 7 and 100 mM KCl, respectively. The data at 100 mM KCl are from Perrella et al. (*3*).

Table 6: Ratio k_2/k_1 of the Rate Constants for CO Binding to the α and β Chains in the First Ligation Step under Various Conditions of pH and Cl^- Concentrations[a]

pH	[Cl^-] (mM)	k_2/k_1
6.2	7, 100	1.24 ± 0.14
7	7	2.05 ± 0.55
7	100	1.47 ± 0.15
8.5	7, 100	2.19 ± 0.35

[a] The ratio was calculated assuming $k_1 \neq k_2$, $k_3 = k_5$, $k_4 = k_6$, $k_7 = k_9 = k_8 = k_{10}$, $k_{11} = k_{12} = 6\ \mu M^{-1}\ s^{-1}$, as in the kinetic model of Figure 8d. The value at pH 7, 100 mM Cl^- was obtained by the analysis of the data from Perrella et al. (*3*).

DISCUSSION

Functional Heterogeneity of Intermediates 21 and 22. As shown in Table 2, the species isolated by cryofocusing a sample of partially oxidized HbCO and identified (first column) by our previously reported procedure (*22, 2*) disproportionate into the expected parental species when refocused at 15 °C (third column). Furthermore, the unstable asymmetric hybrids disproportionate into the same parental species irrespective of the method used for their production: a) an equilibrium solution of 50% oxidized HbCO in which 10 species are present in approximately statistical proportions [Figures 3 (panel d) and 4 (panels a−g)]; b) a nonequilibrium solution obtained by rapidly mixing Hb with CO to yield 50% saturation and by the thermal/chemical quenching to trap the intermediates [Figures 5 (panel a) and 6 (panels a−g)].

Besides confirming the validity of the procedure for the identification of the intermediates, the disproportionation experiments have clarified the nature of the component unresolved by the cryogenic technique. This component, which amounts to no more than 5% of the total in the CO association reactions, contains both intermediates 21 (about 65%) and 22 (about 35%) [Figure 5 (panels b and c) and Table 3]. The slight quantitative difference between the two intermediates was reproducible and, according to the protein assays carried out as controls, not due to a significant interference by the reactions of auto-oxidation, heme exchange, and electron transfer in the course of isolation procedure. The difference in the concentrations of species 21 and 22 indicates that the structurally nonequivalent configurations of the liganded α and β chains endow these intermediates with different kinetic properties in the interactions with CO. This finding is consistent with the thermodynamic study of the same CO intermediates carried out by Huang and Ackers (*23*), which indicates a slight, but significant, difference in the energetics of these species. A difference in functional properties between species 21 and 22 is not consistent with a concerted mechanism of cooperativity and has been the main argument in favor of an alternative interpretation of the mechanism of hemoglobin cooperativity, known as the symmetry rule (*1*). Thus, our work supports the concept that a common basic mechanism underlies all hemoglobin reactions.

The error in the determination of the distributions of intermediates in the CO association reaction does not allow us to calculate the rate constants for CO binding to intermediates 21 and 22. However, the energetics of the intermediates in the deoxy/cyanomet model (see introductory portion of this paper) extended to the intermediates in the CO reactions, suggests the following interpretation of the observed difference in their concentrations. In the second CO binding step, the production of species 21 should be favored kinetically with respect to species 22, 23, and 24 as a result of the cooperativity within the dimeric half-molecule. The species 22, 23, and 24 that might be formed in this step are in the R conformation. They should react with the third CO molecule more rapidly than species 21, which retains the T conformation. Thus, the differences in the rates of formation and further reaction with CO of species 21 and 22, predicted on the basis of the energetics, can explain qualitatively the observed different concentrations of these species in the association reaction.

Modulation of the Association Reaction by Proton and Chloride. Some interesting indications were provided by the analyses carried out at different levels of complexity.

Data Analysis According to the Model of Four Consecutive Reactions. If the slight functional heterogeneity of the chains of the intermediates in the same ligation state is ignored and the data are pooled, as in Figure 7, it can be noted that the distributions of the intermediates (Figure 7, panels a−c) did not conform to those expected for a statistical distribution (Figure 7d) under all the conditions studied. The monoliganded species, particularly at acidic pH, tended to approach the statistical distribution, yet the other species were present in low amounts as a result of the high cooperativity in the reaction. A simple model of four consecutive reactions provides a useful, although approximate, overview of the effects. Using this model, Gibson (*10*) determined a value of the rate constant for the binding of the last CO molecule, $l_4' = 6.0\ \mu M^{-1}\ s^{-1}$, invariant with pH (*11*), from studies of the kinetics of CO rebinding in flash photolysis experiments. By adopting this value we found that the rate constants for the binding of the third CO molecule were approximately invariant under all conditions (Table 4). The data at pH 6.3 and 8.5, where no significant chloride effect was observed, and the data at pH 7 in 100 mM chloride (*3*) indicate that the rates of the binding reactions increase continuously under all conditions (Table 5) and, (a) at acidic pH, no marked acceleration occurs up to the binding of the last CO molecule ($l_2'/l_1' = 1.89$ and $l_3'/l_2' = 2.70$), (b) at neutral pH, the reaction accelerates significantly after the binding of the second ligand molecule ($l_2'/l_1' = 2.34$ and $l_3'/l_2' = 5.55$), and (c) at alkaline pH, the reaction undergoes a marked acceleration after the binding of the first ligand molecule ($l_2'/l_1' = 9.66$ and $l_3'/l_2' = 1.98$). Such accelerations in the reaction rates at neutral and alkaline pH explain the greater overall cooperativity found under these conditions ($l_4'/l_1' =$ 53 and 67, respectively) as compared with that observed at acidic pH ($l_4'/l_1' = 22$).

A simulation of the kinetics assuming a concerted model of quaternary structural transitions (*12*) was carried out using the approach suggested by Hopfield et al. (*13*) (see Materials and Methods for details). The distributions of the intermediates predicted by the model are plotted in Figure 10, panels a and b and are checked against the experimental data in Figure 10a. Assuming the data on *L* from Imai (*17*), Table 1, the predicted distributions of intermediates are close enough to the observed values at pH 6.3 and 7. At alkaline pH, the predicted concentrations of monoliganded species are much larger than those observed at pH 8.5 (Figure 10a). Assuming the data on *L* from Chu and Ackers (*18*), the

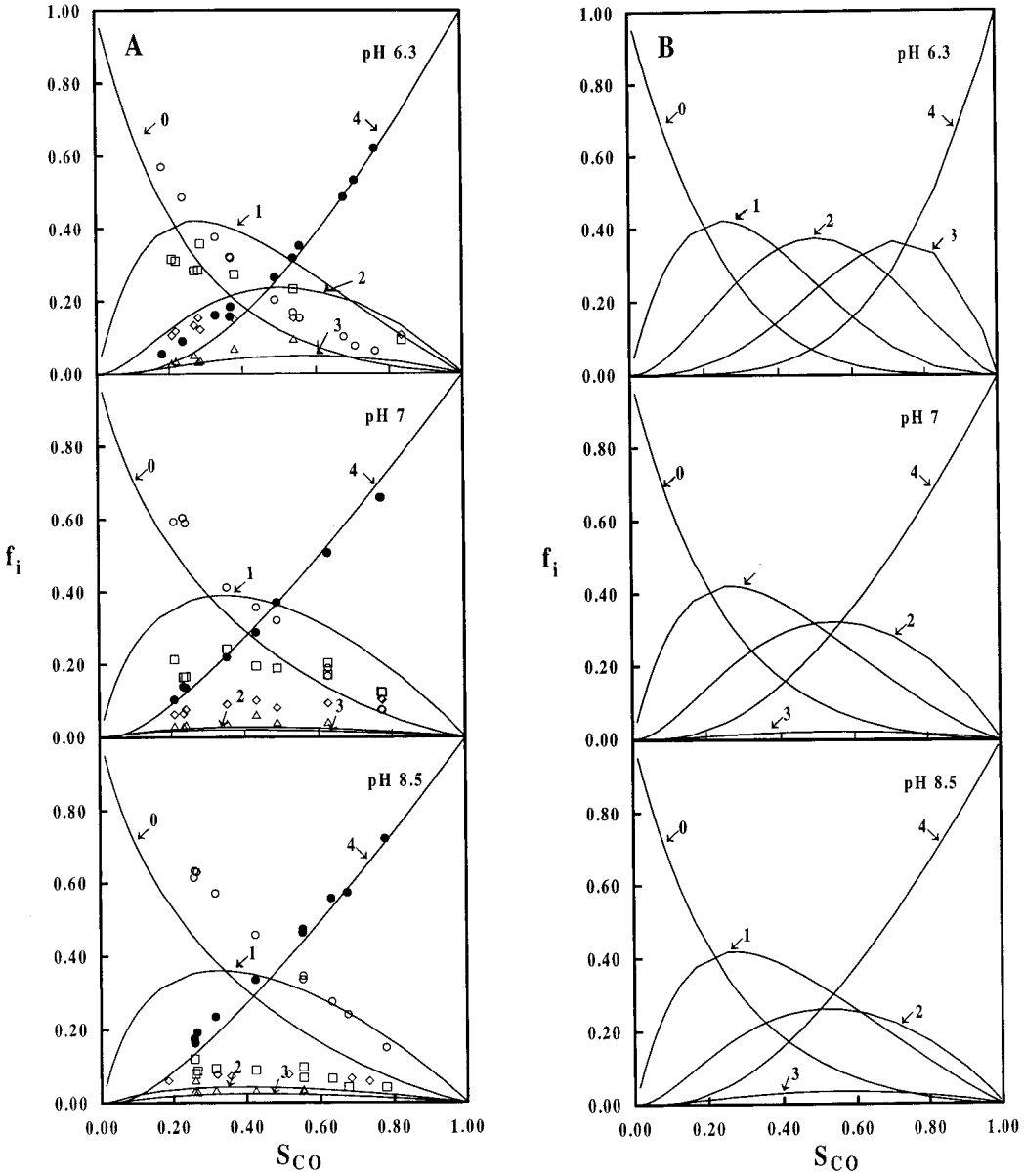

FIGURE 10: Distributions of intermediates generated by the association reactions at pH 6.3, 7, and 8.5, as calculated assuming concerted transitions of quaternary structures at each ligation step [Monod et al. (*12*) and Hopfield et al., (*13*)]. Calculations based on the values of the allosteric constant *L* determined by Imai (*17*) (A), and by Chu and Ackers (*18*) (B), Table 1. The data at pH 6.3 and 8.5 are the data in Figure 7, panels a and c, obtained in 100 mM KCl. The data at pH 7, 100 mM KCl, are from Perrella et al. (*3*). The symbols and arrows are as in Figure 7.

predicted concentrations of diliganded species are larger than the values observed at pH 6.3 and especially at pH 7. At alkaline pH, a much larger population of monoliganded species is predicted than that observed at pH 8.5 (Figure 10b), in agreement with the simulations carried out using the Imai's data. The simulations were also carried out using the values of l_1' from MacQuarry and Gibson (*11*). Statistical distributions of intermediates were predicted under all condition by assuming the values of *L* from Chu and Ackers (*18*) and at alkaline pH assuming the values of Imai (*17*).

In conclusion, ignoring the slight difference in the concentrations of species 21 and 22 reported in this work, which suggests different CO binding kinetics for these intermediates, the two-state model provided a qualitative fit of the observed distributions of intermediates at acidic and neutral pH, despite the approximations contained in the assumptions made for the kinetic simulation and in the various parameters obtained from the literature or extrapolated. Our kinetic simulation agrees with the results of a more sophisticated analysis, including geminate ligand rebinding, carried out by Henry et al. (*24*). At alkaline pH, however, values of *L* several orders of magnitude lower than those determined from equilibrium experiments under similar conditions would fit the experimental data reported in this work. The large discrepancy between the predictions of the two-state model and the experimental observations at alkaline pH suggests that both quaternary and tertiary structural transitions might be involved in the cooperative binding of CO under these conditions. This is not surprising since evidence of the involvement of tertiary and quaternary effects in cooperativity has been obtained also in the nonphysiological case of the cyanomet model of ligation.

The energetics of the deoxy/cyanomet intermediates provides the rationale for a possible interpretation of the

experimental findings, particularly at alkaline pH. The free energy change ΔG_C for the transition from deoxy to fully liganded and to the monoliganded intermediates is about 7.1 and 3.7 kcal/mol at pH 7 and about 3.7 and 2.5 kcal/mol at pH 8.5, respectively (*4*). Thus, at alkaline pH, the energy of the monoliganded state becomes very close in value to that of the R quaternary structure. This phenomenon is not due to a quaternary change in structure of the intermediates, but to a pH-dependent tertiary structural effect within a T quaternary structure. Such a tertiary effect is likely to lower the energy barrier for the binding of the second molecule of ligand. Similar values for the energetics of the oxygen monoliganded intermediates were calculated from oxygen equilibrium experiments (*25*). Thus, it can be predicted from the energetics that the second molecule of CO will react with the monoliganded species faster at alkaline pH than at neutral pH, as observed experimentally.

Data Analysis According to Multiple Pathways of Reaction. Effects of Proton and Chloride. Despite the new information on the nature of the previously unresolved component and the estimate of the relative concentrations of species 21 and 22 in the association reaction at pH 7 in 100 mM chloride, a solution of the general kinetic scheme was not feasible owing to the large error in the data. Thus, the analysis was focused on the specific question of the functional heterogeneity of the α and β chains. The reaction schemes with varying number of constraints, as depicted in Figure 8, agreed in indicating a functional heterogeneity of the α and β chains in the first ligation step under all conditions. The evidence for such a heterogeneity was first produced in our previous work on the CO association reaction at pH 7 in 100 mM KCl (*3*). It was then confirmed by the use of noncryogenic techniques under the same conditions (*26*) and is also supported by studies of CO binding to normal and mutated hemoglobin by the stopped-flow method (*27*, *28*).

The relative values of the rates for the binding of the first CO molecule to the α and β chains listed in Table 6 indicate that chain heterogeneity increased by lowering the proton concentration. A low chloride concentration also appeared to increase chain heterogeneity at neutral pH, although the error does not allow a quantification of the effect. A clear qualitative indication of the different effects of low and high chloride concentrations at neutral pH is given in Figure 9b, which compares the distributions of the monoliganded intermediates under the two conditions. It is interesting that an effect of chloride is apparent at physiological pH, where chloride is expected to act as a modulator of oxygen affinity. Such an effect could be possibly more significant with oxygen as a ligand, as observed with the organic phosphates. Equilibrium NMR studies of the effects of 2,3-DPG and IHP on the partition of the ligand between the α and β chains gave a clear indication of greater O_2 binding to the β chains in the presence of the organic phosphate, whereas such an effect was not observed with CO (*29*). However, the cryogenic technique, as a result of its ability to resolve the mixtures of intermediates, has revealed differences in CO binding to the α and β chains in the presence and in the absence of IHP under dynamic conditions (*3*).

A mechanistic interpretation of the effects of different chloride concentrations on the kinetics of CO binding, namely the lack of any observable effect at pH 6.3 and 8.5 and a slight effect at pH 7, would be speculative since the data are not sufficiently precise. A structural interpretation is complicated by the existence of at least two classes of sites for chloride binding, involving the α-amino group of Val1(α) (*30*, *31*) and the ϵ-amino group of Lys82(β) (*32*), characterized by different affinities for the ligand and pH dependence of the affinities. However, the findings reported here and in other works, quoted above, that chloride, proton and organic phosphate elicit different, or opposite, effects on ligand binding to the α and β chains suggest the possibility that mechanisms of interaction among the modulators of oxygen affinity exist, which could be of significance for the fine-tuning of oxygen delivery to the tissues.

ACKNOWLEDGMENT

We acknowledge gratefully the many illuminating discussions with Gary Ackers and collaborators and the valuable comments by Kim Vandegriff regarding our work.

REFERENCES

1. Ackers, G.K., Doyle, M.L., Myers, D., and Daugherty, M.A. (1992) *Science 255*, 54−63.
2. Perrella, M., and Rossi-Bernardi, L. (1994) *Methods Enzymol. 232*, 445−460.
3. Perrella, M., Davids, N., and Rossi-Bernardi, L. (1992) *J. Biol. Chem. 267*, 8744−8751.
4. Daugherty, M. A., Shea, M. A., and Ackers, G. K. (1994) *Biochemistry 33*, 10345−10357.
5. Perrella, M., Benazzi, L., Ripamonti, M., and Rossi-Bernardi, L. (1994) *Biochemistry 33*, 10358−10366.
6. Shibayama, N., Morimoto, H., and Saigo, S. (1997) *Biochemistry 36*, 4375−4381.
7. Daugherty, M. A., Shea, M. A., Johnson, J. A., LiCata, V. J., Turner, G. J., and Ackers, G. K. (1991) *Proc. Natl. Acad. Sci. U.S.A. 88*, 1110−1114.
8. Ackers, G. K., Perrella, M., Holt, J. M., Denisov, I., and Huang, Y. (1997) *Biochemistry 36*, 10822−10829.
9. Berger, R. L., Davids, N., and Perrella, M. (1994) *Methods Enzymol. 232*, 517−558.
10. Gibson, Q. H. (1959) *Prog. Biophys. Biophys. Chem. 9*, 1−53.
11. MacQuarrie, R., and Gibson, Q. H. (1972) *J. Biol. Chem. 247*, 5686−5694.
12. Monod, J. Wyman, J., and Changeaux, J.-P. (1965) *J. Mol. Biol. 12*, 88−118.
13. Hopfield, J. J., Shulman, R. G., and Ogawa, S. (1971) *J. Mol. Biol. 61*, 425-443.
14. Samaja, M., Rovida, E., Niggeler, M., Perrella, M., and Rossi-Bernardi, L. (1987) *J. Biol. Chem. 262*, 4528−4533.
15. Sharma, V. S., Schmidt, M. R., and Ranney, H. M. (1976) *J. Biol. Chem. 251*, 4267−4272.
16. Sharma, V. S., Bandyopadhyay, D., Berjis, M., Rifkind, J. and Boss, G. R. (1991) *J. Biol. Chem. 266*, 24492−24497.
17. Imai, K. (1982) *Allosteric Effects in Haemoglobin*, Cambridge University Press, Cambridge, U.K.
18. Chu, A. H., and Ackers, G. K. (1981) *J. Biol. Chem. 256*, 1199−1205.
19. Perrella, M., Colosimo, A., Benazzi, L., Ripamonti, M., and Rossi-Bernardi, L. (1990) *Biophys. Chem. 37*, 211−223.
20. Ferrone, F. A., Martino, A. J., and Basak, S. (1989) *Biophys. J. 48*, 269−282.
21. Eaton, W. A., Henry, E. R., and Hofrichter, J. (1991) *Proc. Natl. Acad. Sci. U.S.A. 88*, 4472−4475.
22. Perrella, M., Cremonesi, L., Benazzi, L., and Rossi-Bernardi, L. (1981) *J. Biol. Chem. 256*, 11098−11103.
23. Huang, Y., and Ackers, G. K. (1996) *Biochemistry 35*, 704−718.
24. Henry, E. R., Jones, C. M., Hofrichter, J., and Eaton, W.A. (1997) *Biochemistry 36*, 6511−6528.

25. Chu, A. H., Turner, B. W., and Ackers, G. K. (1984) *Biochemistry 23*, 604−617.
26. Perrella, M., Ripamonti, M., Benazzi, L., and Denisov, I. (1996) *Biophys. Chem. 61*, 169−176.
27. Mathews, A. J., Rohlfs, R. J., Olson, J. S., Renaud, J.-P., Tame, J., and Nagai, K. (1991) *J. Biol. Chem. 266*, 21631−21639.
28. Mathews, A. J., and Olson, J. S. (1994) *Methods Enzymol. 232*, 363−386.
29. Viggiano, G., and Ho, C. (1979) *Proc. Natl. Acad. Sci. U.S.A. 76*, 3673−3677.
30. Chiancone, E., Norne, J. E., Forsen, S. Antonini, E., and Wyman, J. (1972) *J. Mol. Biol. 70*, 675−688.
31. Nigen, A. M., Manning, J. M., and Alben, J. O. (1980) *J. Biol. Chem. 255*, 5525−5529.
32. Bonaventura, J., Bonaventura, C., Sullivan, B., Ferruzzi, G., McCurdy, P. R., Fox, J. and Moo-Pen, W. F. (1976) *J. Biol. Chem. 251*, 7563−7571.

BI971669U